Applied Science and Innovative Research
ISSN 2474-4972 (Print) ISSN 2474-4980 (Online)
Vol. 8, No. 4, 2024
www.scholink.org/ojs/index.php/asir

Original Paper

Analysis of Transient Flow Field and Rock Cuttings Trajectory in Large-Diameter Reaming Drilling

Peishu Li[1,2,3], Ke Gao[1,2,3], Yumin Wen[1,2,3], Yan Zhao[1,2,3*]

[1] College of Construction Engineering, Jilin University, Changchun 130061, China

[2] Key Laboratory of Drilling and Exploitation Technology in Complex Conditions, Ministry of Natural Resources, Jilin University, Changchun 130061, China

[3] Engineering Research Center of Geothermal Resources Development Technology and euipment, Ministry Education, Jilin University, Changchun 130061, China

[*] Corresponding Author: Zhao Yan, E-mail: zhaoyan1983@jlu.edu.cn

Received: October 25, 2024 Accepted: November 17, 2024 Online Published: November 22, 2024

doi:10.22158/asir.v8n4p149 URL: http://doi.org/10.22158/asir.v8n4p149

Abstract

This paper investigates the transient flow field characteristics and rock cuttings trajectory during large-diameter reaming drilling, aiming to address the issue of low debris removal efficiency. By establishing a liquid-solid two-phase flow numerical model, the flow field of a bundled down-the-hole hammer for 830mm reaming drilling was simulated, and the flow velocity, pressure distribution, and rock cuttings movement trajectory within the hole bottom and return channel were analyzed. The study found that the bit rotation significantly influences the flow field, increasing the area of high-speed regions at the hole bottom, enhancing the average flow velocity of the flow field, and facilitating the removal of rock cuttings. Simultaneously, the pressure difference in the flow field at the hole bottom is crucial for transporting rock cuttings to the debris removal pipe, and there exists an optimal critical value of bit rotation speed to achieve the best reverse circulation effect of the flow field. The analysis of rock cuttings trajectory shows that the flow field at the hole bottom can be divided into three stages, with different characteristics of rock cuttings distribution at each stage. Increasing the diameter of the debris removal hole helps enlarge the area of high-speed regions for rock cuttings, improving debris removal efficiency. This study provides theoretical guidance for enhancing debris removal efficiency in large-diameter reaming drilling.

Keywords

Large-diameter reaming drilling, Transient flow field at hole bottom, Rock cuttings trajectory, Liquid-solid two-phase flow, Debris removal efficiency study

1. Introduction

Large-diameter reaming drilling refers to the drilling technology that enlarges an existing wellbore to a larger diameter, with the initial purpose of solving drilling challenges such as wellbore necking and wall collapse. This technology was gradually applied to the field of oil drilling in the early 20th century and later extended to large-diameter drilling incoal seams prone to outbursts, scientific deep drilling, and horizontal directional drilling (HDD) widely used in the laying of pipelines for water supply, electricity, telecommunications, natural gas, and oil, achieving remarkable results. Yan Jianlong and others designed a diamond reaming tool to address necking and collapse issues in the lower wellbore sections after casing wall protection, which does not require casing withdrawal and increases drilling efficiency. Liu Kelin and his team developed the PS-150/700D locally enlarged diameter double-wing reaming bit, which exhibits good stability in locally enlarging the diameter of coalbed methane cavern wells. Tian and his colleagues designed a dual-diameter and dual-speed composite drilling tool that uses a pilot bit to form a pilot wellbore, releasing in-situ stresses, while the reaming bit enlarges the pilot wellbore to the target diameter. They also analyzed the acceleration mechanism of this tool and conducted field tests and numerical simulations on its drilling performance under different diameter ratios and rotational speed combinations. Liu and others established constraint equations for the pin joints of large-diameter coalbed methane reaming tools using Newton-Euler dynamics theory and conducted dynamic simulations, optimizing the pin joints that affect the performance and lifespan of the reaming tools.

According to existing research, studies on large-diameter reaming drilling currently focus primarily on bit structure and drilling tool design, as well as drilling efficiency. As drilling efficiency improves, issues such as repeated rock fragmentation at the bottom of the hole often arise, leading to reduced drilling efficiency. Therefore, this paper focuses on the study of rock cuttings trajectory and flow field characteristics at the bottom of the hole under large-diameter reaming conditions (above 800mm). By conducting dynamic analyses of the wellbore flow field, rock cuttings at the bottom of the hole, and rock cuttings in the central passage, we obtain models for the velocity and pressure distribution of the wellbore flow field and the velocity of rock cuttings at the bottom of the hole under reaming conditions. Fluent is utilized for fluid dynamics simulation analysis to establish a liquid-solid two-phase flow model under large-diameter reaming drilling conditions, providing theoretical guidance for improving the reverse circulation debris removal efficiency in large-diameter reaming drilling.

2. Numerical Model of Liquid-Solid Two-Phase Flow Field in Large-Diameter Reaming Drilling

2.1 Model Establishment and Boundary Condition Setting

The structure of the clustered down-the-hole hammer for 830mm reaming drilling is shown in Figure 1, mainly consisting of a pilot bit, an impactor, and a slag discharge pipe. During the drilling process, the pilot bit first drills into the pilot hole and serves to align and guide the drilling. Subsequently, the impactor, driven by gas, reciprocates downward, while the drilling fluid enters the annulus between the

wellbore wall and the down-the-hole hammer, carrying the rock cuttings from the hole bottom into the slag discharge pipe and ultimately into the upward return channel of the drill pipe, achieving reverse circulation.

The model was imported into Spaceclaim for volume extraction, where the area where the mud flows through was extracted and simplified. The simplified model is shown in Figure 2.2. The annulus between the down-the-hole hammer and the wellbore wall was set as the drilling fluid inlet for the fluid domain, while the end of the upward return channel was set as the drilling fluid outlet, and the end of the drill pipe's upward return channel was also designated as an outlet.

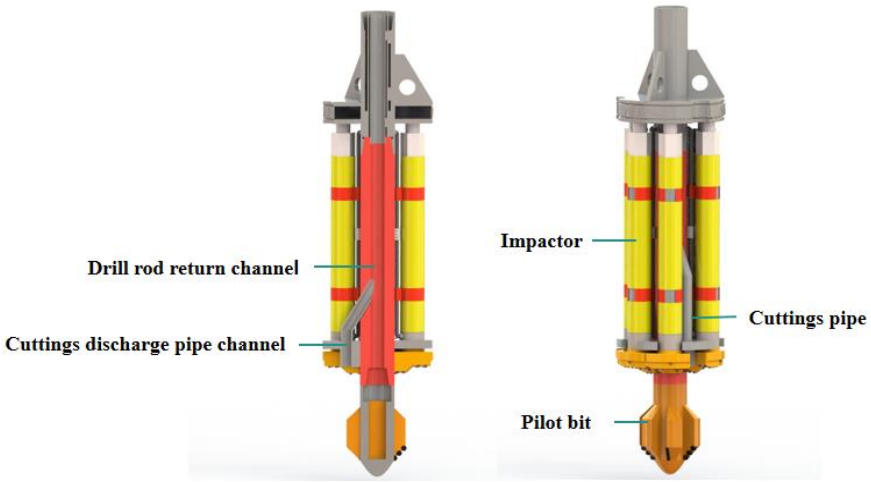

Figure 1. Clustered Down-the-Hole Hammer Model for Large-Diameter Reaming Drilling

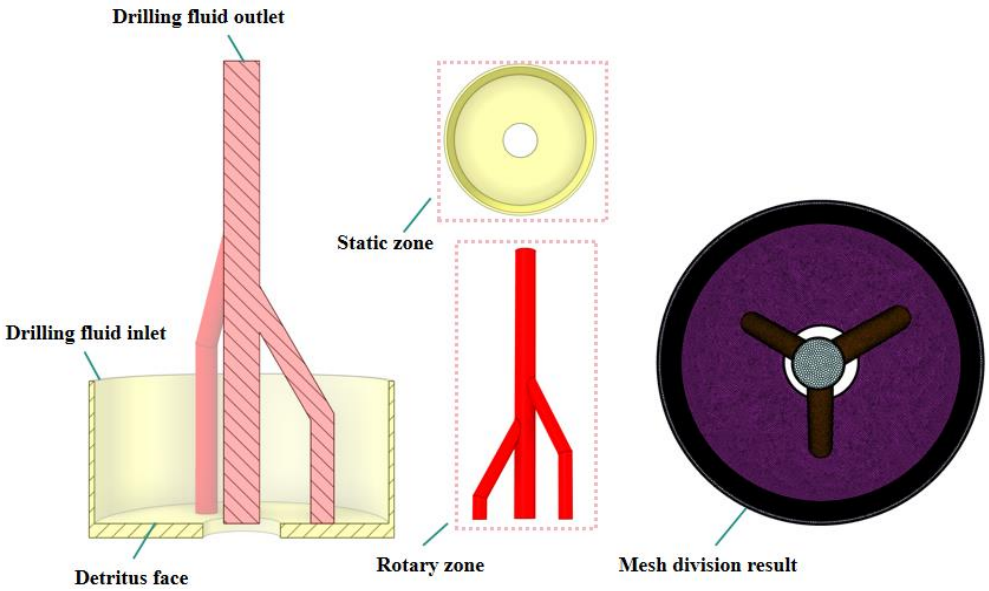

Figure 2. Simplified Fluid Domain and Mesh Division

2.2 Selection of Computational Model and Configuration of Discrete Phase Parameters

Using the DDPM (Dense Discrete Phase Model) within the Eulerian two-phase flow framework for calculations, this model, despite its higher computational cost, offers exceptional accuracy in simulating the discrete phase. It is particularly well-suited for modeling densely distributed discrete phases. Additionally, transient calculations are employed, with the drilling fluid pump rate set to 12.5 L/s and the rotational speed of the rotating region set to 30 rpm. Other parameters remain at their default values. The simulation time for the fluid field is set to 10 seconds. The rock-breaking surface at the bottom of the hole is designated as the rock debris injection surface, with a debris density of 2660 kg/m ^{3} and a mass flow rate of 0.08 kg/s. The debris generation time is set to 10 seconds. During the simulation, the trajectories of the rock debris, as well as the dynamic changes in velocity and pressure at the bottom of the hole and within the debris discharge pipe, are recorded in real-time. The specific boundary condition parameters are shown in Table 1 below

Table 1. Boundary Condition Parameters Table

Parameters	value
Pump Rate of Drilling Fluid (L/s)	30
Rotational Speed of the Rotating Area(rpm)	30
Mass Flow Rate of Rock Debris(kg/s)	0.08
Density of Rock Debris(kg/m3)	2660
Simulation Time of Fluid Field(s)	10

3. Analysis of Transient Flow Field in Large-Diameter Reaming Drilling

Addressing the unclear understanding of the flow field variations in large-diameter reaming drilling operations, a numerical simulation of the liquid-solid two-phase flow in the entire flow field of large-diameter reaming drilling was conducted. This study explored the flow field variations within the bottom-hole flow field and the return channel flow field, as well as the transient flow field changes within the debris discharge pipe during the reverse circulation process. The aim was to comprehensively reveal the flow field variation patterns in large-diameter reaming drilling, providing a theoretical basis for subsequent analyses to improve debris removal efficiency.

3.1 Analysis of Transient Flow Field in the Return Channel and Debris Discharge Pipe

In the simulated flow field lasting for 10 seconds, the flow field gradually stabilizes after 5 seconds. Upon observing the velocity contour of the flow field in the return channel and debris discharge pipe after stabilization (Figure 3), it can be found that during large-diameter reaming drilling, the flow velocity at the bottom of the hole is relatively low, with a velocity of 0.21 m/s away from the debris discharge pipe, while the velocity near the entrance of the debris discharge pipe is higher, reaching 1.43 m/s at the entrance. When the fluid flows into the debris discharge pipe, due to the smaller pipe

diameter, a higher flow velocity is formed at this point. The maximum flow velocity mainly occurs in the vertical section of the debris discharge pipe, reaching 1.91 m/s. After the fluid flows into the debris discharge pipe, due to centrifugal force, the fluid velocity accelerates, and there are significant differences in fluid velocity distribution. The velocity is higher near the upper wall of the debris discharge pipe and lower near the lower wall. After passing through the inclined section of the debris discharge pipe, the fluid converges at the return channel. The velocity distribution in the return channel is relatively uniform, with the overall velocity increasing. The velocity at the outlet reaches 1.67 m/s, and the maximum velocity, which is 1.70 m/s, occurs near the center of the outlet.

Observing the changes in the flow field from 0.2 seconds to 10 seconds (Figure4), it is found that the overall flow velocity gradually increases with time and then stabilizes. The main reason is that in the initial stage of the flow field, the rotation has a minor impact on the flow field. As the rotation time increases, the overall flow velocity of the flow field also increases slightly due to the rotation. Over time, the flow field exhibits periodic changes and gradually stabilizes.

To observe the velocity variation within the return channel, a measurement line is set along the centerline of the return channel. The velocity distribution along the measurement line is shown in Figure 5. The maximum velocity occurs at the outlet, reaching 1.62 m/s. The overall flow velocity shows an increasing trend and stabilizes at 1.62 m/s near the outlet. The flow velocity at the bottom of the return channel is very low, with a velocity of only 0.1 m/s at the 400mm position. There is a significant acceleration of the fluid between 400mm and 600mm. The main reason is that two shorter debris discharge pipes converge in this area, causing a substantial increase in flow velocity due to the convergence of a large amount of fluid in this region.

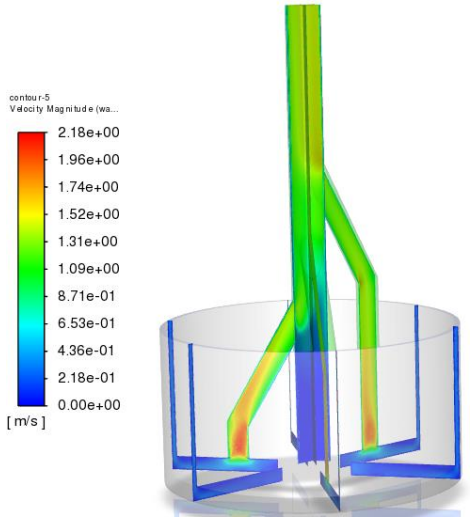

Figure 3. Velocity Distribution in the Return Channel and Debris Discharge Pipe After Flow Field Stabilization

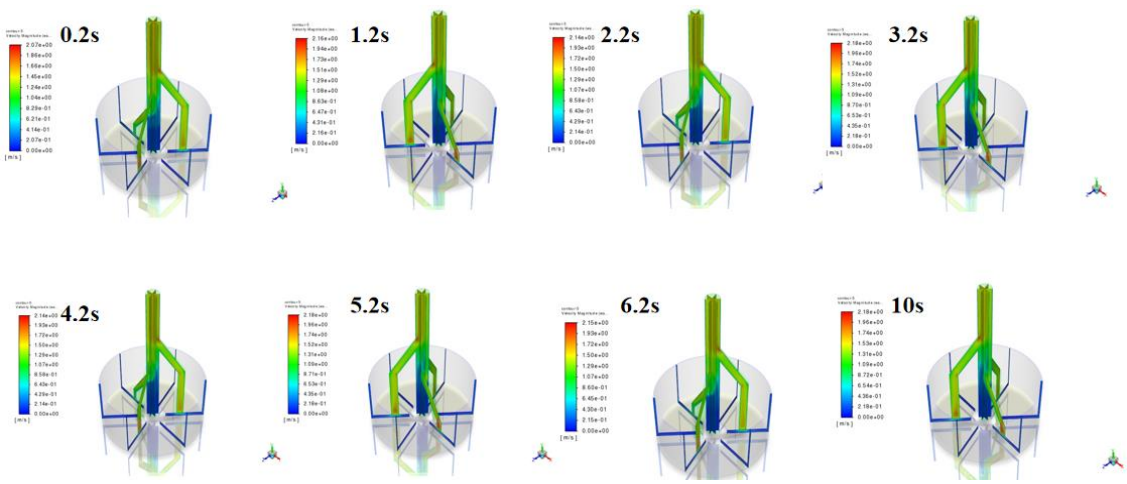

Figure 4. Flow Field Variation Process in the Return Channel and Debris Discharge Pipe within 10 Seconds

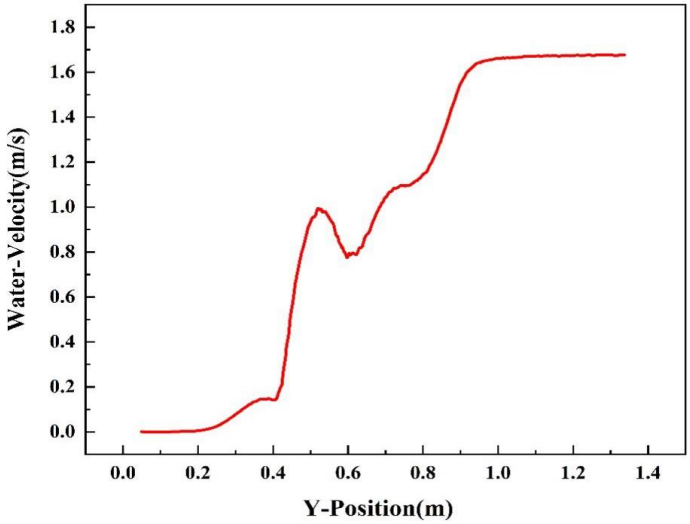

Figure 5. Velocity Variation Curve in the Return Channel

Within the region from 500mm to 600mm, the flow velocity decreases, and only after 600mm does the velocity increase further. Observing the flow field trace diagram (Figure 6), it can be seen that a low-speed vortex is induced by the rotation of the drill pipe in the region from 500mm to 600mm. Therefore, the fluid velocity decreases significantly at this stage. Consequently, an excessively large space below the drill pipe is detrimental to the development of the overall flow field. After 600mm, due to the convergence of the longest debris discharge pipe and the return channel, the flow velocity increases further and eventually stabilizes at approximately 1.62 m/s.

To observe the velocity distribution within the debris discharge pipes in detail, three measurement lines were first set up along the centerlines of the inclined sections of the three debris discharge pipes. The velocity distribution curves, as shown in Figure 7, reveal that within the inclined sections of the debris discharge pipes, the pipe with the shortest vertical height of 300mm exhibits the highest velocity close

to the vertical section, reaching 1.7 m/s. This is advantageous for transporting cuttings into the return channel. Conversely, the debris discharge pipe with a vertical height of 500mm has the lowest velocity at the entrance of its inclined section, measuring only 1.44 m/s, while the corresponding velocity at the 700mm pipe is 1.54 m/s. Comparing the velocities at the ends of these pipes, it is evident that the longer the inclined section, the more developed the flow field and the greater the velocity at the end. Therefore, the debris discharge pipe with a vertical height of 700mm has the highest velocity at the end of its vertical section, reaching 1.86 m/s, while the 300mm pipe has the lowest velocity of 1.60 m/s. Overall, the velocities within the vertical sections show a trend of first decreasing and then increasing. The primary reason for this is that the fluid is continually accelerating in the latter half of the pipe. The longer the pipe, the greater the final velocity of the fluid. Additionally, near the end of the inclined section of the debris discharge pipe, there is a corner, and the fluid velocity tends to increase as it approaches this corner.

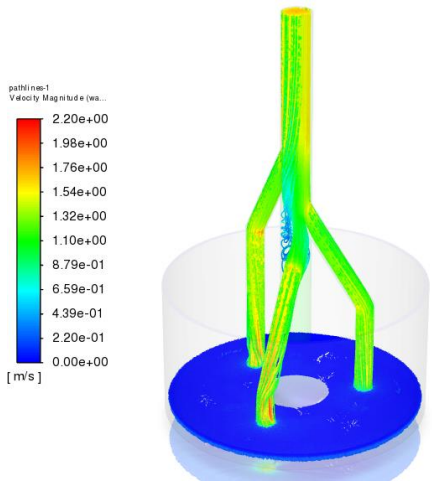

Figure 6. Flow Field Trace Diagram within the Return Channel

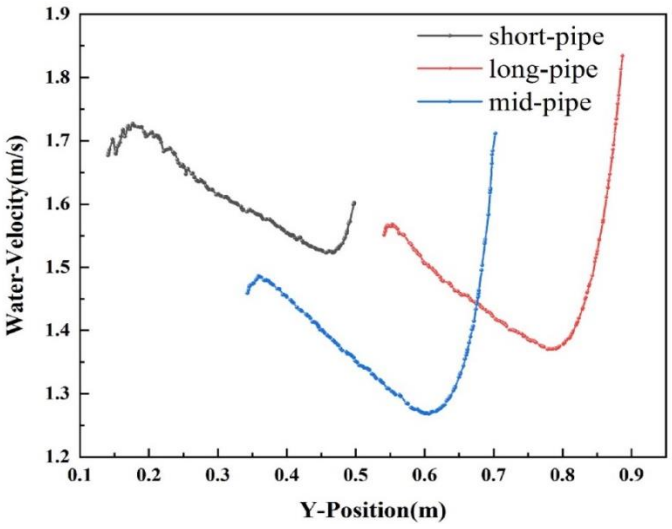

Figure 7. Velocity Distribution Curve in the Inclined Section of the Debris Discharge Pipe

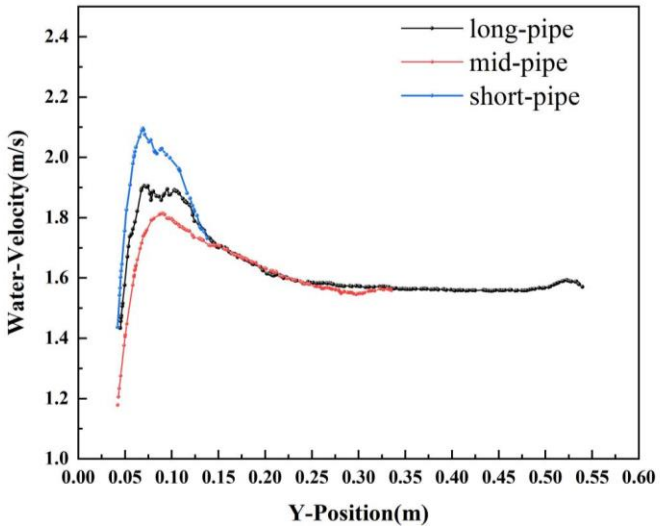

Figure 8. Velocity Distribution Curve in the Vertical Section of the Debris Discharge Pipe

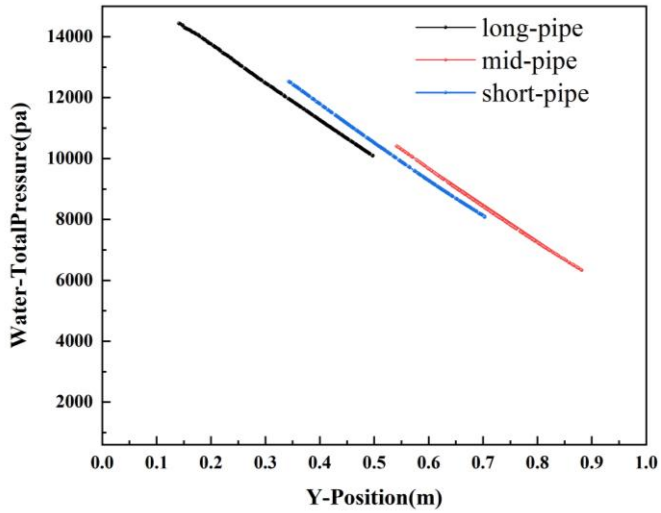

Figure 9. Total Pressure Distribution Curve in the Inclined Section of the Debris Discharge Pipe

Observing the total pressure distribution curves in the inclined sections of the three debris discharge pipes (Figure 9), it can be seen that the total fluid pressure decreases linearly within the pipes. Additionally, the shortest debris discharge pipe exhibits the highest total pressure, with a pressure of 14,500 Pa at the start of its inclined section. By examining the static pressure contour plot of the return channel (Figure 10), it is evident that the total pressure increases as one approaches the bottom of the hole. Furthermore, the pressure always decreases linearly within the pipe where the pipe diameter remains constant. Therefore, it is hypothesized that reducing the length of the inclined section of the debris discharge pipe can effectively decrease the pressure loss within the pipe and enhance the reverse circulation effect of the flow field.

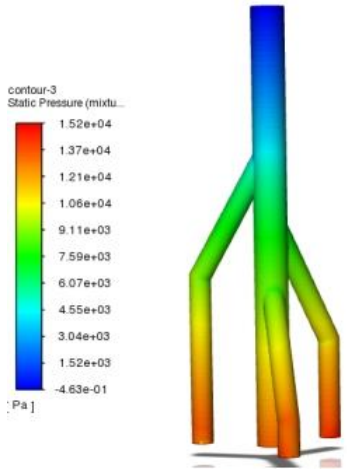

Figure 10. Pressure Contour Plot within the Return Channel

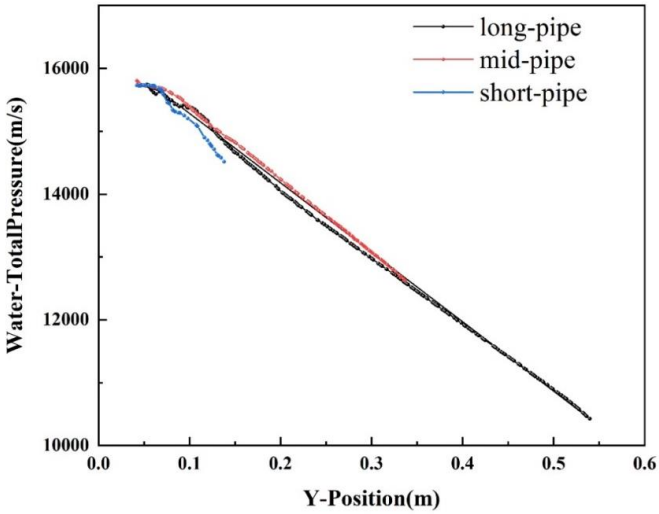

Figure 11. Total Pressure Distribution Curve in the Vertical Section of the Debris Discharge Pipe

3.2 Analysis of Transient Flow Field at the Bottom of a Hole

The primary issue leading to inefficient debris removal lies in the timely discharge of rock cuttings hindered by repeated rock fragmentation at the bottom of the hole. Therefore, studying the variation patterns of the flow field at the bottom of the hole during large-diameter reaming drilling is crucial. To this end, during the simulation of the flow field over 10 seconds, we recorded the velocity and pressure distribution at the bottom of the hole in real-time to observe changes in the flow field's velocity and pressure during the drilling process.

After the flow field stabilized, by observing the velocity distribution of the flow field at the bottom of the hole (Figure 12), we found that the velocity was highest at the debris removal hole, reaching a maximum of 0.62 m/s. A high-velocity zone formed along the diameter near the debris removal hole, with velocities around 0.4 m/s. Rock cuttings in this high-velocity zone are more easily entrained into

the debris removal channel compared to those in other areas. Therefore, increasing the area and velocity of this zone will directly enhance the speed of debris removal at the bottom of the hole.

By observing the velocity changes in the flow field at the bottom of the hole over 10 seconds (Figure 13), we noticed that as the drill bit rotated longer, its impact on the flow field gradually increased. Initially, the high-velocity zone was small and concentrated near the debris removal hole, with a circumferential distribution. As the drill bit continued to rotate, the high-velocity zone gradually expanded and extended towards the center of the drill pipe, changing its shape to an irregular, nearly circumferential form. Three distinct low-velocity zones, with velocities of about 0.02 m/s, emerged near the center of the drill pipe. This may lead to some accumulation of rock cuttings. However, as rotation continued, the previous low-velocity zones evolved into high-velocity zones connected to the high-velocity zone at the debris removal hole, which somewhat prevented complete accumulation of rock cuttings in these areas. This indicates that the rotation of the drill pipe and bit plays a significant positive role in rapid debris removal at the bottom of the hole. Furthermore, as the duration of the flow field increased, this effect on the flow field became increasingly apparent.

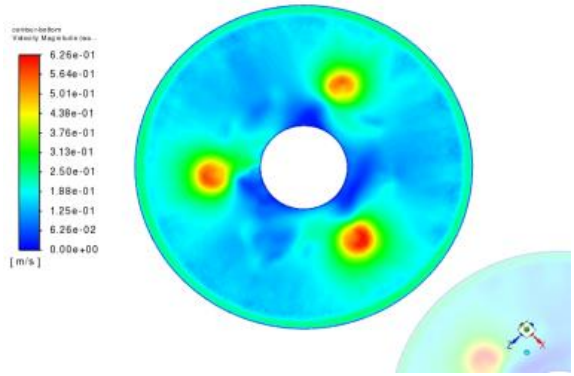

Figure 12. Velocity Distribution of the Flow Field at the Bottom of the Hole at 10 Seconds

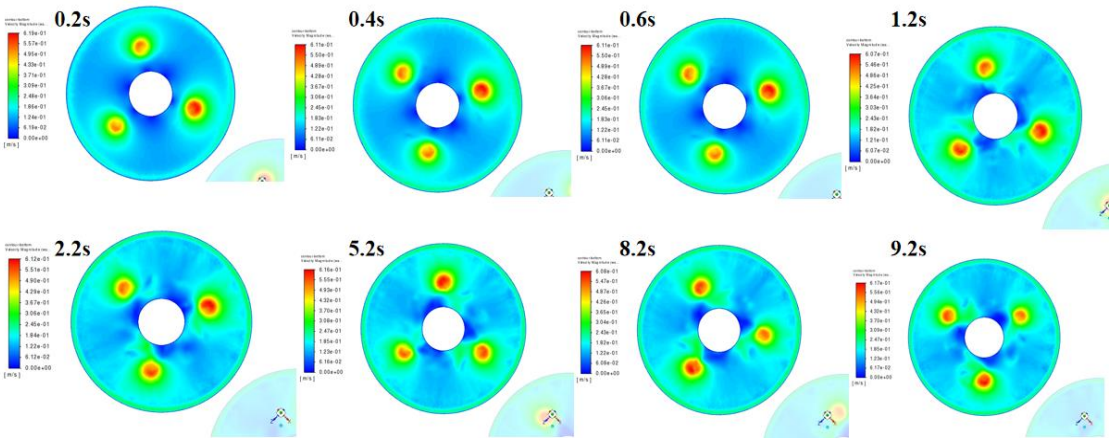

Figure 13. Velocity Variation of the Flow Field at the Bottom of the Hole within 10 Seconds

To further elucidate the characteristics and changes of the flow field at the bottom of the hole, an analysis of both static pressure and total pressure at the bottom of the hole was conducted. Observing the contour plot of static pressure at the bottom of the hole (Figure 14), it can be noted that the static pressure at the debris removal hole is approximately 15,800 Pa. A significant high-pressure zone appears around the debris removal hole, with the highest pressure reaching 16,300 Pa, creating a pressure difference of approximately 400 Pa. Increasing this pressure difference will facilitate the better transport of rock cuttings into the debris removal pipe. In the contour plot of static pressure, the high-pressure zone corresponds to the low-velocity zone near the center of the drill pipe in the aforementioned flow field at the bottom of the hole. Enlarging the area of this high-pressure zone while reducing the maximum static pressure value will be beneficial for the removal of rock cuttings.

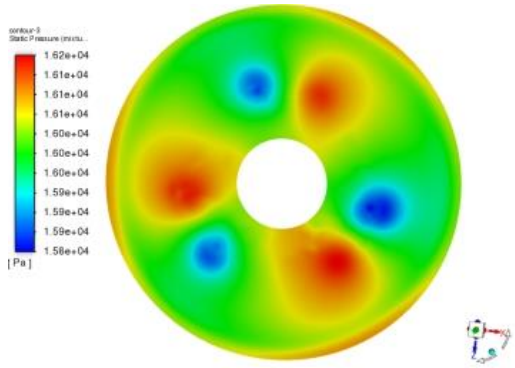

Figure 14. Static Pressure Contour of the Flow Field at the Bottom of the Hole at 10 Seconds

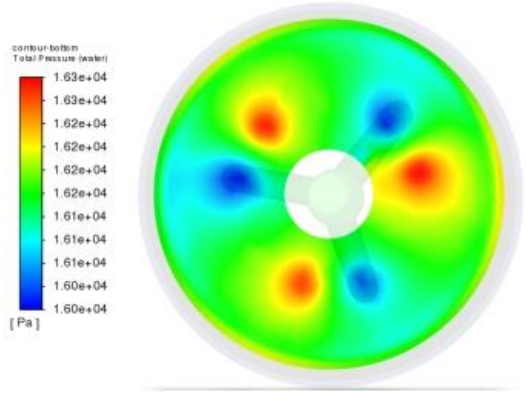

Figure 15. Total Pressure Contour of the Flow Field at the Bottom of the Hole at 10 Seconds

Observing the contour plot of total pressure at the bottom of the hole (Figure 15), it can be noted that the total pressure is minimum at the debris removal hole, approximately 16,000 Pa. The highest total pressure occurs in the low-velocity zone surrounding the debris removal hole. The emergence of this high-pressure zone is primarily due to the stirring effect of the rotating drill bit on the flow field at the bottom of the hole. Fluid that was about to be discharged from the bottom of the hole at the previous

moment fails to be expelled in time due to changes in the position of the debris removal hole. Therefore, this fluid that is not expelled in time forms a high-pressure zone in this area. The area of this high-pressure zone is similar to the area of the debris removal hole, leading to the speculation that the diameter or cross-sectional area of the debris removal hole is a direct factor influencing the area of the high-pressure zone. Additionally, there is a certain distance between the high-pressure zone and the low-pressure zone, which is mainly determined by the rotational speed of the drill pipe and drill bit. The slower the rotational speed of the drill bit, the closer this distance, which is more conducive to the timely discharge of fluid carrying rock cuttings. However, a slower rotational speed of the drill bit also results in a smaller area of high-velocity zones at the bottom of the hole, which is unfavorable for the smooth initiation of rock cuttings. Therefore, it is speculated that there exists a critical rotational speed for the drill bit and drill pipe, and when this critical speed is reached, the overall reverse circulation effect of the flow field is optimal.

4. Study on the Transport Trajectory of Rock Cuttings in Large-Diameter Reaming Drilling

To gain a more intuitive understanding of the transport patterns of rock cuttings in large-diameter reaming drilling, the motion trajectories of the rock cuttings in the return channel and at the bottom of the hole are recorded in real-time during the simulation. Analyzing these transport patterns provides theoretical support for efficient debris removal in large-diameter reaming drilling.

4.1 Analysis of Rock Cutting Transport Trajectory in the Return Channel and Debris Removal Pipe

By observing the trajectories of rock cutting transport in the flow field within 10 seconds and recording key time points, it was found that during the initial stage of the flow field (0s-0.8s), as shown in Figure 16, the rock cuttings mainly moved within the debris removal pipe with a velocity of approximately 0.8 m/s and concentrated near the upper wall of the pipe. This was primarily because the high-velocity fluid region at this time was also concentrated near the upper wall of the debris removal pipe. A small amount of rock cuttings settled in the lower space around the drill pipe, where their movement speed was very slow, approximately 0.2 m/s, corresponding to the lower fluid velocity in the 400mm-600mm region mentioned above. This indicated that an excessively large space around the lower drill pipe was not conducive to the timely removal of rock cuttings. As time progressed, after 1.2 seconds, the rock cuttings gradually entered the return channel and began to ascend in a spiral motion along the outer wall of the drill pipe, with their velocity gradually increasing to 1.1 m/s. At this point, the rock cuttings discharged from the three debris removal pipes gradually converged and moved continuously together within the return channel, with the convergence point concentrated at the outlet of the longest debris removal pipe. They were tightly and continuously arranged along the direction of the outlet of the longest debris removal pipe and were ultimately discharged at the outlet, where the velocity of the rock cuttings increased to a maximum of 1.4 m/s.

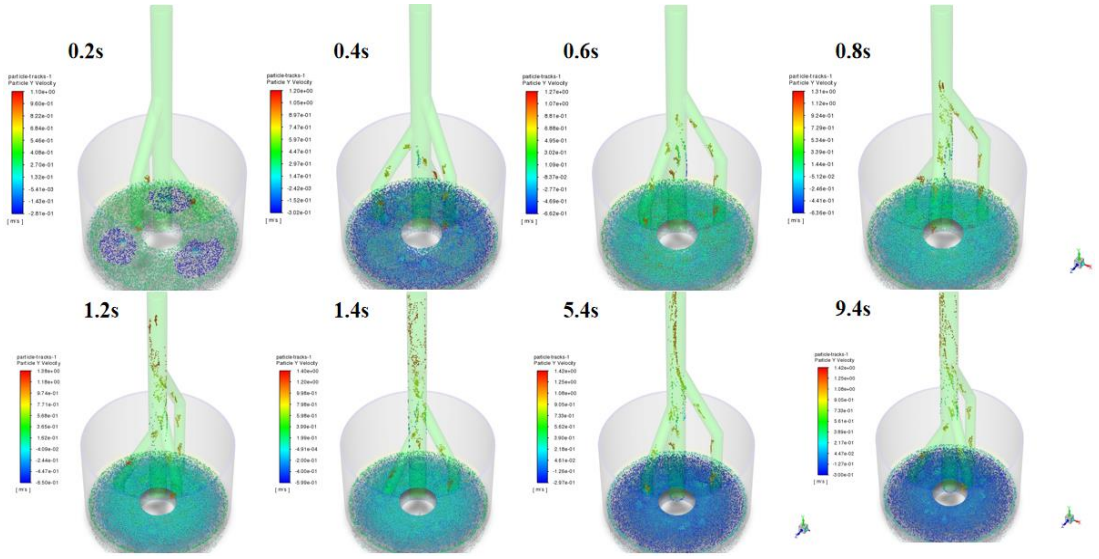

Figure 16. Velocity Contour Plot of Rock Cutting Transport Trajectory within 10 Seconds

4.2 Analysis of Rock Cutting Transport Trajectory at the Bottom of the Hole

The ability to quickly remove debris from the bottom of the hole directly affects the efficiency of debris removal. Therefore, by recording the transport trajectories of rock cuttings at the bottom of the hole and analyzing their movement patterns, we aim to provide a theoretical basis for the theory of rapid debris removal from the bottom of the hole.

To more clearly describe the transport trajectories of rock cuttings at the bottom of the hole, the flow field at the bottom of the hole is divided into three stages based on the different characteristics of the distribution of rock cuttings over time: the initial stage of the flow field (0s-2.2s), the middle stage of the flow field (2.4s-5.6s), and the final stage of the flow field (5.8s-10s).

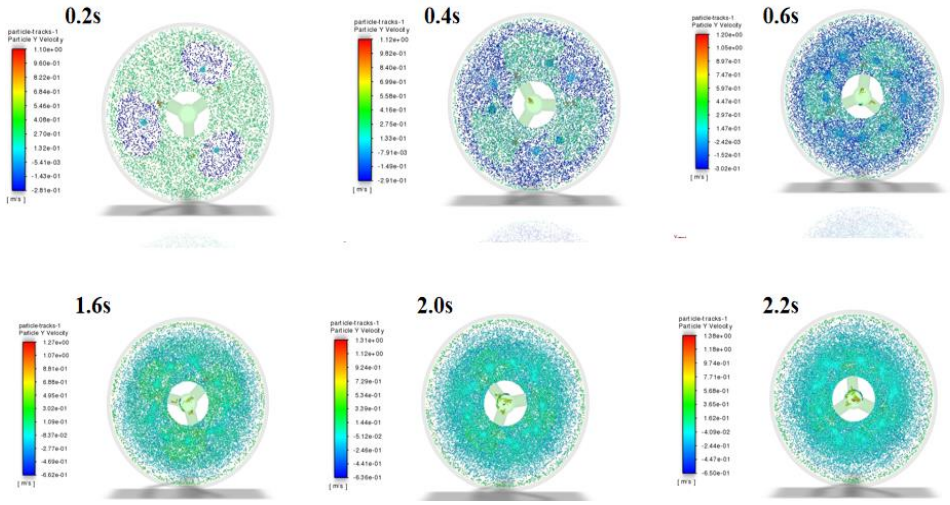

Figure 17. Velocity Contour of Rock Cutting Transport Trajectory in the Initial Stage of the Flow Field

In the initial stage of the flow field, as shown in Figure 17, rock cuttings are first generated uniformly on the rock-breaking surface. The velocity of the cuttings near the debris removal holes begins to increase, and the cuttings that start moving first exhibit a fan-shaped distribution at the bottom of the hole, with a movement speed of 0.3 m/s in this area. As the drill bit rotates, the "fan-shaped" area also rotates, and after 1.6 seconds, the surrounding cuttings gradually start moving under the action of the fluid. A circular high-speed movement area of cuttings gradually appears along the circumference where the debris removal holes are distributed, with the cuttings moving at a speed of 0.43 m/s in this region. As time progresses, the characteristics of this circular area become increasingly clear and distinct.

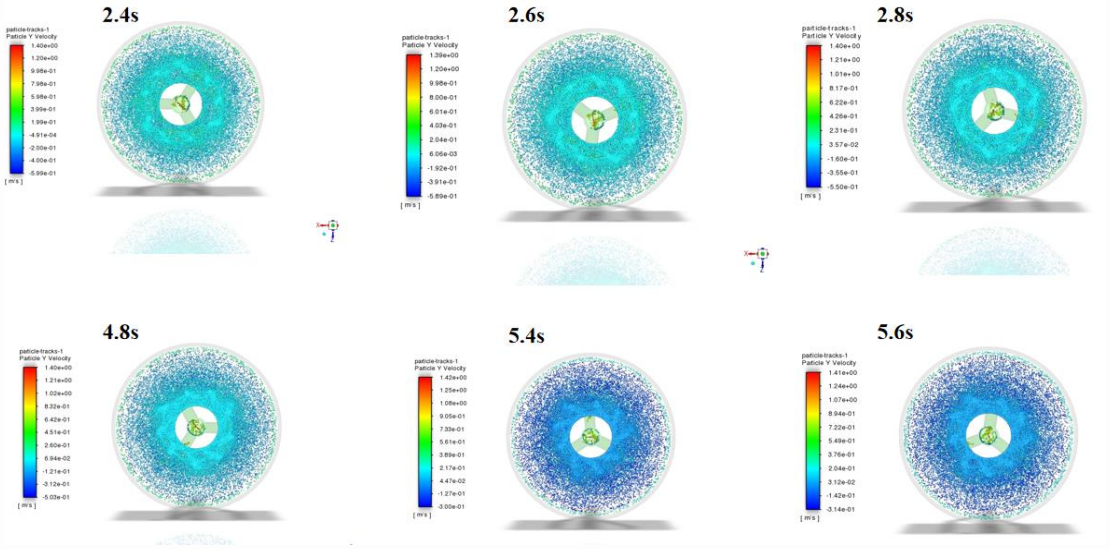

Figure 18. Velocity Contour of Rock Cutting Transport Trajectory in the Middle Stage of the Flow Field

In the middle stage of the flow field (Figure 18), the area of the circular high-speed movement region of rock cuttings further increases, but most of the rock cuttings at the bottom of the hole still accumulate in the gap between the wellbore wall and the drill bit, with speeds ranging from 0.2 m/s to 0.4 m/s. Additionally, aggregation of rock cuttings begins to occur in the circular region, where their speeds are distributed between 0.4 m/s and 0.5 m/s, and a gear-shaped distribution pattern gradually emerges.

In the final stage of the flow field (Figure 19), the circular high-speed movement region of rock cuttings begins to take an irregular, nearly circular shape, indicating that the turbulence level in the flow field at the bottom of the hole is increasing, which is more conducive to the removal of rock cuttings. However, the area of the high-speed region does not further increase and is mainly concentrated within the circle formed by the debris removal holes. Therefore, considering increasing

the distribution diameter of the debris removal holes can effectively enlarge the area of the high-speed region for rock cuttings, facilitating the smooth removal of rock cuttings.

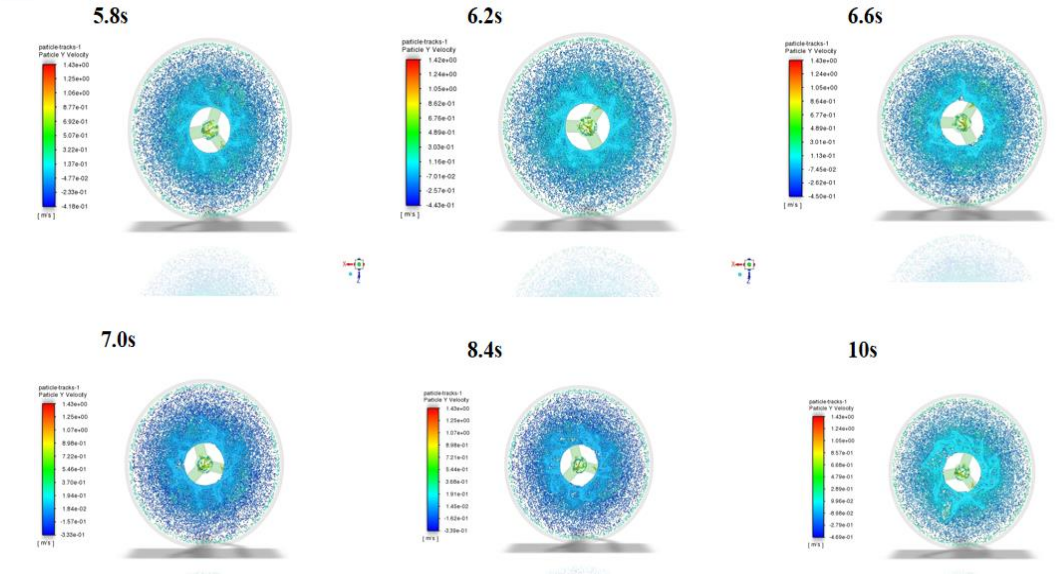

Figure 19. Velocity Contour of Rock Cutting Transport Trajectory in the Final Stage of the Flow Field

5. Conclusion

This paper addresses the challenge of low drilling efficiency due to difficult debris removal in large-diameter reaming operations by analyzing the flow field characteristics and rock cutting transport trajectories under such conditions. During the simulation of the flow field over 10 seconds, the flow velocity and pressure distribution at the bottom of the hole were recorded in real-time, and the transport trajectories of rock cuttings within the flow field were analyzed. The following conclusions were drawn:

(1) The rotation of the drill bit increases the area of the high-speed region and enhances the average flow velocity in the flow field at the bottom of the hole, which is beneficial for rapid debris removal. A pressure difference of approximately 400 Pa forms around the debris removal holes, and increasing this pressure difference facilitates better transportation of rock cuttings into the debris removal pipe. Due to the rotation of the drill bit, high-pressure and low-pressure zones are generated at the bottom of the hole. Reducing the rotational speed decreases the distance between these zones, which is advantageous for debris removal. Therefore, it is speculated that there exists an optimal critical rotational speed.

(2) Excessive space at the lower end of the drill pipe can lead to the formation of low-speed vortices at this location, reducing the flow velocity and diminishing the effectiveness of the reverse circulation. The flow velocity in the longest debris removal pipe is the fastest, having the most significant impact on the flow field.

(3) Based on the different characteristics of rock cutting distribution at the bottom of the hole over time, the flow field at the bottom of the hole is divided into three stages: the initial stage of the flow field (0s-2.2s), where rock cuttings exhibit a fan-shaped distribution; the middle stage of the flow field (2.4s-5.6s), where the area of the high-speed circular movement region of rock cuttings further increases, and a gear-shaped distribution pattern gradually emerges; and the final stage of the flow field (5.8s-10s), where the high-speed circular movement region of rock cuttings begins to take an irregular, nearly circular shape, mainly concentrated within the circle formed by the debris removal holes. Therefore, increasing the distribution diameter of the debris removal holes can effectively enlarge the high-speed area for rock cuttings, facilitating smooth debris removal.

References

Cai Chenggong, & Zhou Gezhong. (2004). Experimental Study on Gas Drainage from Coal Seams by Automatic Variable Diameter Large Diameter Drilling. *Coal Science and Technology, 32*(12), 39-41.

Chen Lin, Wang Lihong, & Zhang Panlong. (2016). Development and Application of a Variable Diameter Stabilizer for One-Trip Drilling in Horizontal Wells. *Oilfield Equipment, 45*(7), 87-89.

Dewey, C. (2012). *Focused Approach to Solving Deepwater Reaming Problems*. Presented at the IADC/SPE Drilling Conference and Exhibition, San Diego, California, USA, 6-8 March 2012. https://doi.org/10.2118/151733-MS

Jing, J., Lu, Y. Y., Zhu, X. H., et al. (2018). Weight Distribution Characteristics During the Process of Hole Enlargement in Drilling. *Arabian Journal for Science and Engineering*, *43*, 6445-6459. https://doi.org/10.1007/s13369-018-3233-z

Liu Kelin, Zhang Zhigang, & Wang Xiaoqin. (2014). Development of a Locally Enlarged Diameter Bi-wing Reaming Bit. *Exploration Engineering*, *41*(3), 48-51. https://doi.org/10.1016/S1876-3804(14)60004-5

Liu, S. L., Liu, R., Zhang, X. H., et al. (2012). Stress Optimization of Coupling Pins for Large Diameter Reaming Tool of Coal-bed Methane Well. *Transactions of the Canadian Society for Mechanical Engineering*, *36*, 1-21. https://doi.org/10.1139/tcsme-2012-0001

Panayirci, H. M. (2019). Hole Enlargement by Drillstring Stabilizers. *Journal of Petroleum Science and Engineering*, *180*, 22-30. https://doi.org/10.1016/j.petrol.2019.04.077

Qian Wen, Qiu Xiaofeng, Su Desheng, et al. (2015). Development and Application of a Mechanical Under-reaming Tool for Drilling Small-Diameter Wells. *Oilfield Equipment*, *44*(1), 60-62.

Qing Shanmeng, Chen Ying, & Zhou Wei. Development of a New Hydraulic Under-reamer.

Tian, J. L., Hu, X. H., Dai, L. M., et al. (2020). Working Mechanism and Experimental Study of Dual-Diameter and Bi-speed Composite Drilling Tool. *International Journal of Green Energy*, *17*(6), 363-372. https://doi.org/10.1080/15435075.2020.1739691

Xin Xinping, Guo Fanjin, & Wei Guoying. (1998). Automatic Variable Diameter Reaming Tool. *Coal Engineers*, *1*, 20-22.

Yang Ying. (2019). Analysis of Patent Technologies for Hole Enlargement in the Oil and Gas Industry. *China Invention & Patent*, *16*(2), 69-74.

Zhao Jiangpeng. (2015). Application of Air Drilling in Coal Mine Rescue Drilling Tunnel Construction. *Coal Technology*, *34*(12), 182-184.

Zhao Yong. (2016). *Design and Mechanical Analysis of a Large Diameter Variable Diameter Reaming Bit for Steering Drilling in Coal Mining*. Chengdu: Master's Thesis, Southwest Petroleum University.

Zhu Xiaohua, & Yi Qinjian. (2018). Study on Rock Fragmentation Efficiency of Bi-cone Reamer for Horizontal Directional Drilling. *Journal of Basic Science and Engineering*, *26*(5), 1130-1139.